Laser-induced thermal grating effects in flames

Skip Williams,* Larry A. Rahn, Phillip H. Paul, and Jon W. Forsman†

Combustion Research Facility, Sandia National Laboratories, Livermore, California 94551

Richard N. Zare

Department of Chemistry, Stanford University, Stanford, California 94305

Received May 9, 1994

Light scattering from a laser-induced thermal grating produced in an atmospheric-pressure H_2/O_2 flame is observed with a phase-matching geometry commonly used in resonant four-wave mixing and laser-induced grating spectroscopy. The presence of thermal gratings is confirmed in both the time and the frequency domains in two distinct experiments. Diluting the flame with helium decreases the thermal grating signal intensity. Experimental results agree well with calculations based on a solution of the linearized hydrodynamic equations.

A laser-induced thermal grating is formed in an absorbing medium from the interference of two copolarized fields, $\mathbf{E}_1$ and $\mathbf{E}_2$, of frequency $\omega = 2\pi c/\lambda$ that cross at a small angle θ.[1] This interference produces a spatial modulation in the laser field intensity in the medium with a spatial period $\Lambda = \lambda/2\sin(\theta/2)$. When the laser frequency is tuned to a resonant spectroscopic transition, a density modulation results from the localized absorption of the laser energy and subsequent heating of the medium. This density modulation leads to a modulation in the (real) refractive index and, hence, forms a thermal grating that can scatter light from a third field, $\mathbf{E}_3$, into a fourth (the signal) field, $\mathbf{E}_4$. Laser-induced thermal gratings have been observed in liquids[2,3] and in solids.[4] These effects might be expected to be small because of the relatively low densities encountered in atmospheric-pressure, high-temperature gases (e.g., flames). We have found that thermal gratings can be produced in flames under some conditions. This observation is consistent with other gas-phase experiments recently reported.[5]

In this Letter we investigate the temporal and spectral characteristics of laser-induced thermal gratings in a flame. In the time-domain experiments, $\mathbf{E}_1$ and $\mathbf{E}_2$ are supplied from a cw ring-dye laser that was pulse amplified by a single-mode Nd:YAG-pumped dye amplifier. The laser output was frequency doubled in KD*P to produce laser beams at ~307–308 nm having pulse widths of ~20 ns and bandwidths of ~0.001 cm^{-1}. The scattering field, $\mathbf{E}_3$, was derived from the frequency-doubled output of a separate multimode Nd:YAG laser operating at 532 nm with a pulse width of ~6 ns. In the experiment the $\mathbf{E}_1$ and $\mathbf{E}_2$ laser frequency was held constant at the line center of the $Q_1(3)$ transition of the OH $A^2\Sigma^+ - X^2\Pi$ (0,0) band, and we determined the temporal response of the thermal grating by delaying $\mathbf{E}_3$ with respect to $\mathbf{E}_1$ and $\mathbf{E}_2$. In the frequency-domain experiments $\mathbf{E}_1$ and $\mathbf{E}_3$ are supplied from the same high-resolution, pulse-amplified laser system and field $\mathbf{E}_2$ is produced from a separately tunable, but otherwise similar, pulse-amplified laser system. In the experiment we probe the spectral response by detuning $\mathbf{E}_2$ from $\mathbf{E}_1$ and $\mathbf{E}_3$, which are maintained at the line center of the $Q_{21}(3)$ transition of the OH $A^2\Sigma^+ - X^2\Pi$ (0,0) band. In this experiment all fields are overlapped in time.

We made the measurements in the postflame gases of a 40-mm-diameter H_2-O_2 flat-flame burner using gas flows of 4.8 standard liters per minute (slm) H_2 and 3.0 slm O_2. The spectra were recorded at a height of 5 mm above the burner surface, which corresponds[6] to a temperature of ~1460 K and an OH concentration of $\sim 2 \times 10^{15}$ molecules/cm^3. Each field is linearly polarized, collimated, and apertured to produce a Gaussian beam profile with a FWHM diameter of 1 mm. Typical UV field intensities were 1.9 and 19 kW/cm^2 for the $Q_1(3)$ and $Q_{21}(3)$ transitions, respectively, which are smaller than one tenth of the calculated saturation intensities.[7] The visible (532-nm) field is nonresonant; therefore saturation is not an issue; however, it does contribute to the background of scattered light. We found that 532-nm energies in the range of 0.3–1 mJ and beam diameters of slightly less than 1 mm produced good signal-to-noise ratios. All signals were detected with a photomultiplier, digitized, averaged over 30–60 laser shots, and stored on a computer for further analysis.

The light scattered from a laser-induced thermal grating is directly proportional to the square of the perturbation in the real part of the refractive index, Δn_R^2, which scales directly as the square of the perturbation in the gas density, $\Delta\rho^2$. For small perturbations the fluctuation in density is given by a solution of the linearized hydrodynamics equations. Taking the laser intensity to be described by the product of a grating in space with some temporal envelope, $L(t)$, and the conversion of laser energy to thermal energy by a cascaded set of linear first-order rate equations, one can approximate the grating signal by

$$I_4 \propto \left\{ [\exp(-t/\tau_{\mathrm{th}}) + A\exp(-t/\tau_{\mathrm{ac}}) \times \cos(2\pi f_{\mathrm{ac}} t + \phi)] * [L(t) * Z(t)] \right\}^2, \quad (1)$$

0146-9592/94/211681-03$6.00/0

where the asterisk denotes the Laplace convolution operator, $f_{ac} = c_0/\Lambda$, and the parameters A and ϕ can be determined directly from the full solution of the problem. The term $Z(t)$ represents the solution to the system of rate equations and has the form of a linear sum of exponential decays, the amplitudes and arguments specifying decay rates, and branching of energy between internal and external modes. In the limit of $(\gamma - 1)(4\pi^2\nu/c_0\Lambda)^3 << 1$, the decay times and the characteristic acoustic frequency are given by

$$\tau_{th} = \Lambda^2 Pr/4\pi^2\nu, \quad (2)$$

$$\tau_{ac} = (\gamma - 1 + 4Pr/3)\Lambda^2 \mathrm{Pr}/2\pi^2\nu. \quad (3)$$

Here Pr is the Prandtl number, ν is the kinematic viscosity, $\gamma = c_p/c_v$ is the heat capacity ratio of the gas, and $c_0 = (\gamma RT/M)^{1/2}$, where R is the ideal gas constant, T is the temperature, and M is the average molecular weight of the gas.

For common gases at moderate pressures (0.1–20 atm) and temperatures (300–5000 K), $0.65 < \mathrm{Pr} < 0.85$ and $1.1 < \gamma < 1.7$. Thus Pr and γ are essentially constant for a large range of gas compositions, temperatures, and pressures. Alternatively, $\nu \propto T^{3/2}M^{-1}$ and $c_0 \propto T^{1/2}M^{-1/2}$. Therefore the temporal decay and the acoustic oscillation of the thermal grating signal are sensitive primarily to the gas composition, the gas temperature, and the grating spacing. For times longer than the appearance of the first maximum, the first term in brackets in relation (1) can be used to fit experimental data, in which case the observed values of τ_{ac}, A, and ϕ will depend strongly on the exact details of the energy deposition process as well as on the convolution with a probe laser of finite width.

Figures 1(a) and 1(b) show time-delay spectra for two different crossing angles θ between the copolarized grating forming fields $\mathbf{E}_1$ and $\mathbf{E}_2$ corresponding to two different grating spacings, i.e., $\Lambda = 44.3 \pm 8.9$ μm ($\theta = 0.398° \pm 0.080°$) and $\Lambda = 13.3 \pm 0.9$ μm ($\theta = 1.33° \pm 0.09°$), respectively. The data of Fig. 1(a) were fitted to relation (1), giving values of $\tau_{th} = 115 \pm 3$ ns, $\tau_{ac} = 57 \pm 3$ ns, and $1/f_{ac} = 46.9 \pm 0.4$ ns. With the use of the flame temperature of 1460 K and assuming that combustion is complete at 5 mm above the burner surface (hence the gas consists of 89% H_2O and 11% O_2), we calculate that $\tau_{th} = 109 \pm 43$ ns, $\tau_{ac} = 185 \pm 76$ ns, and $1/f_{ac} = 50.8 \pm 10.2$ ns, using the values $\mathrm{Pr} = 0.7161$, $\gamma = 1.223$, $\nu = 3.258 \times 10^{-4}$ m^2/s, and $c_0 = 871.33$ m/s. The transport properties were determined by standard procedures[8] for the measurement conditions. The large error in the calculated values is the result of the uncertainty in the determination of the grating spacing. Nevertheless, the disagreement between the calculated and the fitted values for τ_{ac} is well outside the expected error.

Figure 1(a) shows the results of a calculation of the thermal grating signal, based on a formal solution to the linear hydrodynamics equations, for two different energy thermalization mechanisms. The dashed curve corresponds to a one-step model in which electronically excited OH is quenched by H_2O and all the energy is converted to translation. The solid curve corresponds to a two-step model in which 20% of the energy is converted to translation by the electronic quenching with the balance converted into H_2O internal energy (first step). The H_2O internal energy is then converted to translation (second step) at a rate seven times slower than that for OH quenching. The particular values for this rate and the partition of energy were determined by the best fit to the data. The two calculations demonstrate that the acoustic modulation of the thermal grating signal is dramatically affected by the details of the energy deposition mechanism and that reproducing the data requires a two-step model. The thermal grating shown in Fig. 1(b) decays approximately 11 times faster than the thermal grating of Fig. 1(a). The theoretical curve shown in Fig. 1(b) was obtained with the same two-step energy deposition model.

The forward phase-matching geometry used in our experiments is commonly used in nearly degenerate and degenerate four-wave mixing[9] (NDFWM and DFWM) and laser-induced grating spectroscopy.[10] Specifically, if the grating forming fields $\mathbf{E}_1$ and $\mathbf{E}_2$ are of the same (or nearly the same) frequency, then the thermal grating, NDFWM, DFWM, and laser-induced grating spectroscopy signals all propagate along the same phase-matched direction, i.e., they have the same Bragg-scattering angle. In a previous paper[11] one of us showed how polarization measurements can be used to determine whether thermal gratings are contributing to the DFWM signal. In addition, it was suggested that polarization configurations in which $\mathbf{E}_1$ and $\mathbf{E}_2$ are cross polarized discriminate against thermal gratings because fields

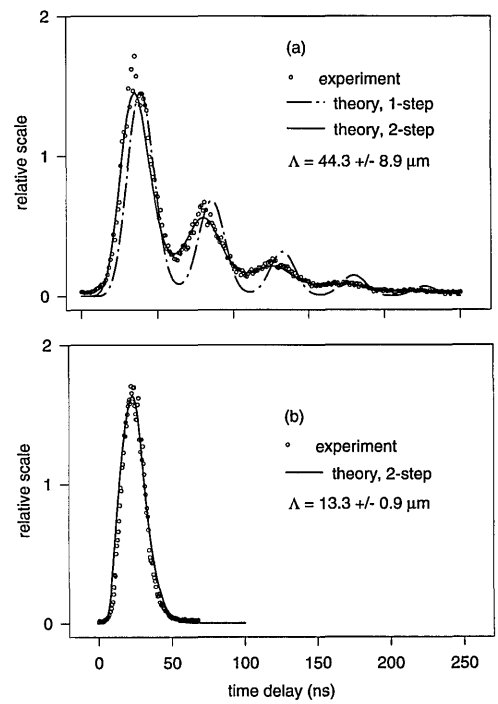

Fig. 1. Thermal grating time dependence. Scattered light intensity of $\mathbf{E}_4$ versus time delay of $\mathbf{E}_3$ with respect to $\mathbf{E}_1$ and $\mathbf{E}_2$. Time $t_0 = 0$ corresponds to the rising edge of the UV laser pulses. The dashed–dotted and solid curves are the results of full calculations with the one- and two-step mechanisms, respectively.

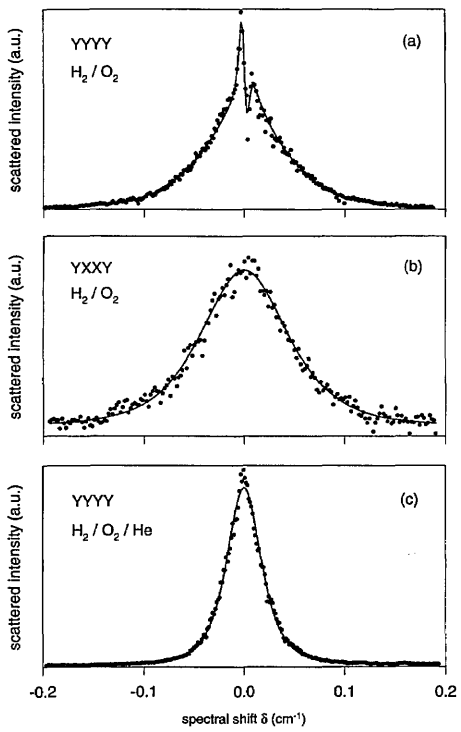

Fig. 2. Thermal grating spectral dependence. Scattered light intensity of $\mathbf{E}_4$ versus spectral shift of $\mathbf{E}_2$ relative to $\mathbf{E}_1$ and $\mathbf{E}_3$. X and Y denote orthogonal linear polarization states, and the polarization of the fields is given in the order $\mathbf{E}_4\mathbf{E}_1\mathbf{E}_3\mathbf{E}_2$. The grating spacing for all spectra is $\Lambda = 5.9 \pm 0.3$ μm. The solid curves are only a guide to the eye.

with orthogonal polarizations do not produce a spatial modulation of the field intensity (only a spatial modulation in field polarization).[10]

Figures 2(a) and 2(b) show NDFWM spectra for two different polarization configurations. In Fig. 2(a) $\mathbf{E}_1$ and $\mathbf{E}_2$ are copolarized and can produce a thermal grating, and in Fig. 2(b) $\mathbf{E}_1$ and $\mathbf{E}_2$ are cross polarized and thus cannot produce a thermal grating. Note that a narrow (long-lived) feature superimposed upon a broader line shape is present in Fig. 2(a) but absent in Fig. 2(b). In addition, the narrow feature is dispersive, indicating coherent interference and a $\pi/4$ phase shift with respect to the underlying NDFWM signal. This phase shift results from the fact that the thermal grating contribution arises from a perturbation to the real refractive index. The dispersive line shape corresponds to a lifetime of ~1 ns. With Eq. (2), the calculated thermal decay time is $\tau_{th} \sim 2$ ns for $\Lambda = 5.9$ μm. These times are much longer than the homogeneous relaxation time ($1/\Gamma$) of the $Q_{21}(3)$ population in this flame of 0.09 ns,[7] which accounts for the fact that the thermal grating line shape appears narrow compared with the underlying NDFWM line shape. The relative amplitudes of the narrow and broad features indicate the relative strengths of the thermal and NDFWM grating signals, respectively.

Diluting the flame with helium at 14.54 slm greatly diminishes the thermal grating signal relative to the NDFWM signal. The reduction of the thermal grating signal in the helium-diluted flame is supported by the absence of the narrow feature in the spectrum of Fig. 2(c) recorded with $\mathbf{E}_1$ and $\mathbf{E}_2$ copolarized. The underlying NDFWM line is narrower because of a reduced relaxation rate in the He-diluted environment. The temperature of the $H_2/O_2/He$ flame 5 mm above the burner is only 80 K (5%) lower than in the H_2/O_2 flame; however, the gas composition is now 3.0% O_2, 24% H_2O, and 73% He, which dramatically changes the kinematic viscosity, speed of sound, and index of refraction of the medium.

We have shown that high-temperature gases at atmospheric pressure are capable of generating strong thermal gratings under some conditions and that the thermal grating signal depends on fundamental real gas parameters such as the temperature and the composition. In this study both the gas composition and the temperature were known, and it was possible to model the temporal behavior of the thermal grating signal. Conversely, the observation of a thermal grating should permit the determination of the speed of sound from time-domain measurements of the acoustic frequency and hence the temperature in a gas of known composition.

This research was funded by the U.S. Department of Energy, Basic Energy Sciences, Division of Chemical Sciences, and the U.S. Air Force Office of Scientific Research. S. Williams gratefully thanks Department of Energy and the U.S. Air Force Office of Scientific Research.

*Present address, Division of Chemical Science and Technology, MS G755, Los Alamos National Laboratory, Los Alamos, New Mexico 87545.

†Present address, Laboratoire de Physique Moleculaire, Université de Franche-Comte, Cedex, France.

References

1. R. Trebino, E. K. Gustafson, and A. E. Siegman, J. Opt. Soc. Am. B **3,** 1295 (1986).
2. H. Eichler and H. Stahl, J. Appl. Phys. **44,** 3429 (1973).
3. R. J. D. Miller, R. Casalegno, K. A. Nelson, and M. D. Fayer, Chem. Phys. **72,** 371 (1982).
4. J. R. Salcedo and A. E. Siegman, IEEE J. Quantum Electron. **QE-15,** 250 (1979).
5. D. E. Govoni, J. A. Booze, A. Sinha, and F. F. Crim, Chem. Phys. Lett. **216,** 525 (1993).
6. J. E. M. Goldsmith, in *20th Symposium (International) on Combustion* (Combustion Institute, Pittsburgh, Pa., 1984), p. 1331.
7. M. S. Brown, L. A. Rahn, and T. Dreier, Opt. Lett. **17,** 76 (1992).
8. R. J. Kee, G. Dixon-Lewis, J. Warnatz, M. E. Coltrin, and J. A. Miller, "A FORTRAN computer code for the evaluation of gas-phase multicomponent transport properties," Rep. Sand86-8246.UC-32 (Sandia National Laboratories, Livermore, Calif., 1986).
9. R. L. Abrams, J. F. Lam, R. C. Lind, D. G. Steel, and P. F. Liao, in *Optical Phase Conjugation,* R. A. Fisher ed. (Academic, New York, 1983), Chap. 8, p. 211.
10. H. J. Eichler, P. Gunter, and D. W. Pohl, in *Laser-Induced Dynamic Gratings* (Springer-Verlag, Berlin, 1986), Chap. 4, p. 94.
11. L. A. Rahn and M. S. Brown, Opt. Lett. **19,** 1249 (1994).